


MUFASA: Timescales for H_I consumption and SFR depletion of satellite galaxies in groups

Mika Rafieferantsoa^{1,2,3} [†], Romeel Davé^{4,1,2,5}, Thorsten Naab³

¹ University of the Western Cape, Bellville, Cape Town 7535, South Africa

² South African Astronomical Observatory, Observatory, Cape Town 7925, South Africa

³ Max-Planck-Institut für Astrophysik, D-85748 Garching, Germany

⁴ Institute for Astronomy, Royal Observatory, Edinburgh EH9 3HJ, UK

⁵ African Institute for Mathematical Sciences, Muizenberg, Cape Town 7945, South Africa

Last updated 2017 July 6; in original form 2017 July 6

ABSTRACT

We investigate the connection between the H_I content, SFR and environment of galaxies using a hydrodynamic simulation that incorporates scaling relations for galactic wind and a heuristic halo mass-based quenching prescription. We run two zoom-in simulations of galaxy groups with $M_{\text{halo}} > 10^{13} M_{\odot}$ at $z = 0$, selected to have quiet merger histories. We track galaxies as they become satellites, and compute the delay time τ_{d} during which the satellites are similar to central galaxies at a given stellar mass, and a fading time τ_{f} during which satellites go from gas-rich and star-forming to gas-poor and quiescent. We find $0.7 \lesssim \tau_{\text{d}} \lesssim 3$ Gyr at $z = 0$, and depends inversely on the satellite halo mass at infall. At $z \sim 1$ we find $\sim 0.3 \lesssim \tau_{\text{d}} \lesssim 2$ Gyr, broadly consistent with a positive correlation with the Hubble time. For a given halo mass, lower stellar mass galaxies at infall time have higher τ_{d} . We generally find $\tau_{\text{f}} \ll \tau_{\text{d}}$, ranging between ~ 150 Myr at $z \sim 0$ and ~ 80 Myr at $z \sim 1$ based on linear interpolation, with some uncertainty because they are smaller than our simulation output frequency (200 – 300 Myr). τ_{f} has no obvious dependency on infall halo mass. Both timescales show little difference between H_I depletion and SF quenching, indicating that using up the gas reservoir by star formation without refilling is the main mechanism to transform satellite galaxies at these halo masses. At a given physical distance from the center of the main halo of interest, higher redshift galaxies have on average higher cold gas content, but the ratio of gas (H_I or H₂) to star formation rate is similar, indicating that star formation is consistently fed through reservoirs of H_I then H₂. For a given amount of H_I, galaxies have shorter consumption times in more massive halo structures. Our results suggest that group-scale simulations naturally yield a delayed-then-rapid satellite quenching scenario as inferred from observations both today and at earlier epochs, though we highlight some quantitative discrepancies.

Key words: galaxies: evolution – galaxies: statistics – methods: N-body simulations

1 INTRODUCTION

Gas inflow is the main fuel for *in-situ* star formation in galaxies. The current understanding of galaxy evolution stipulates that star formation-driven feedback ejects some of the infalling gas to regulate stellar growth, while feedback associated with black hole accretion prevents gas from reaching massive central galaxies in haloes to quench galaxies (Somerville & Davé 2015; Naab & Ostriker 2017). In addition to these processes, the immediate (e.g. Weinmann et al. 2006; Lacerna et al. 2018) or extended (e.g. Kauffmann et al. 2013;

Rafieferantsoa & Davé 2018) environment of galaxies can also affect their growth. It has long been argued theoretically that the cold gas content of galaxies is ram pressure-stripped when galaxies move at high velocities through a dense medium within a massive host halo (Gunn & Gott 1972). Furthermore, the extended diffuse gas around the galaxies can be removed by the hot gaseous environment of dense structures such as galaxy groups or clusters (Larson et al. 1980). Observations of neutral hydrogen being stripped from satellites in groups and clusters directly support such claims (e.g. van Gorkom et al. 2003; van Gorkom 2004).

Star formation of galaxies is apparently destined to end for galaxies moving within dense environments. An interesting question to examine is the timescale on which such quenching of star formation happens, for various types of galaxies, as this can provide

* Contact e-mail: rafieferantsoamika@gmail.com

† South African Astronomical Observatory, Observatory Road, Cape Town 7925, South Africa

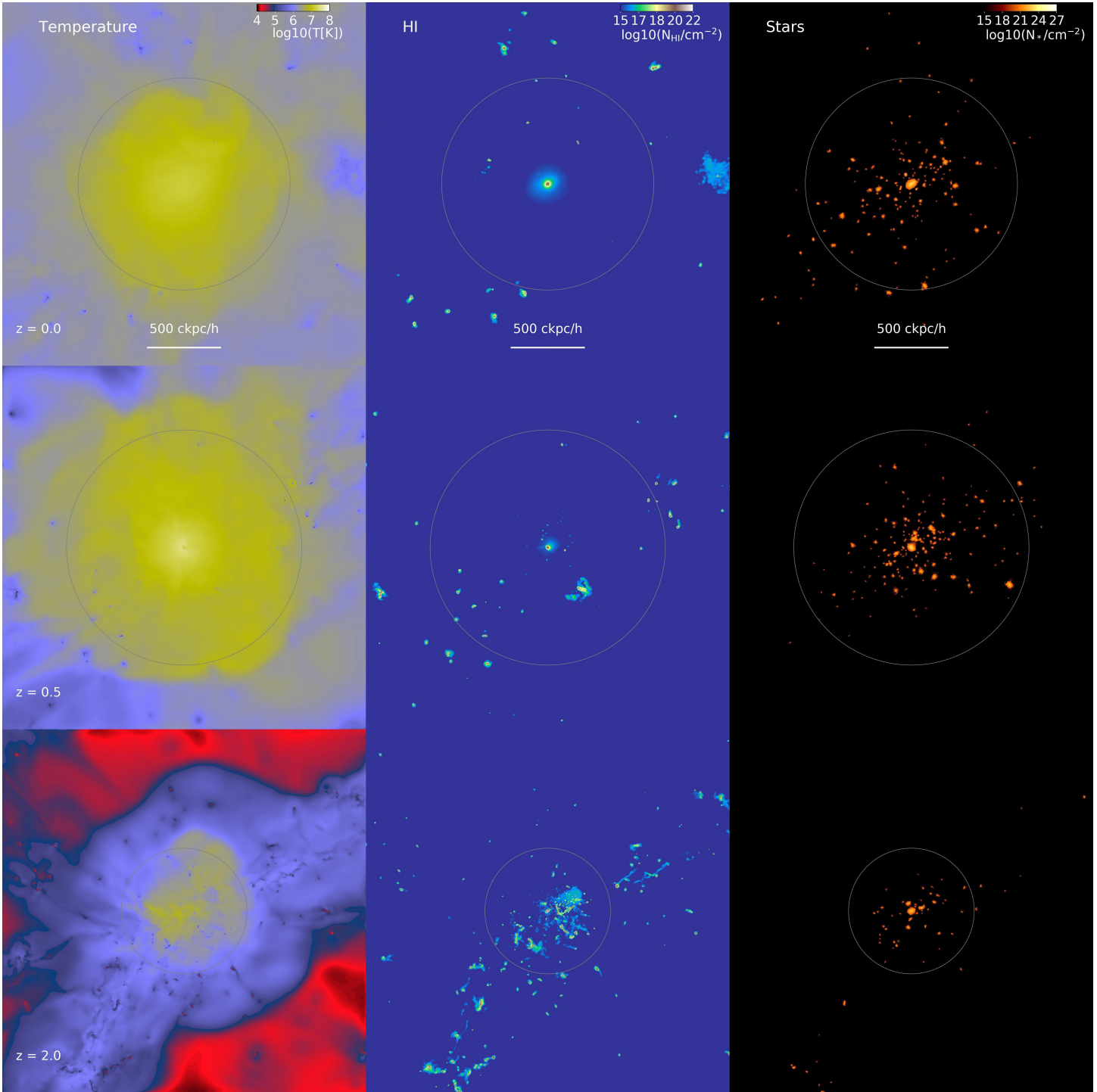


Figure 1. H I at different redshift (*rows*. *Left* columns show the temperature of the gas, *center* for the H I number column densities and the *right* the star particles. The panels are centered at the central galaxy. Although H I is present in the central galaxy at $z = 0$, it does not form stars.

insights into the responsible physical mechanisms. The enormous amount of data provided by the Sloan Digital Sky Survey (SDSS) has permitted many studies of the effects of galaxy environments on the star formation quenching timescales in the nearby Universe. [Kauffmann et al. \(2004\)](#) used SDSS data to analyse the correlation between star formation history and different observed time indicators such as the 4000 break strength and the Balmer-absorption

index $H\delta_A$, and found no dependence with environment, indicating a star formation timescale not less than 1 Gyr. [Peng et al. \(2010\)](#) used SDSS with zCOSMOS ([Lilly et al. 2007](#)) to disentangle two different quenching mechanisms. First, the *environment quenching* –star formation quenching related to the location of the galaxies – is less of a function of redshift out to $z \sim 1$, which they argued to be a consequence of the formation of large-scale structure that leads to

the end of star formation of over half of the satellite galaxies. Second, *mass quenching* – star formation quenching tied to the stellar mass of galaxies – was found to vary on a shorter timescale and is proportional to the star formation rate of the galaxies. [Hirschmann et al. \(2014\)](#) estimated a timescale of ~ 5 Gyr for nearby low mass satellite galaxies seen within SDSS, suggesting a very long quenching time. Recently, [Fossati et al. \(2017\)](#) extended these results to higher redshifts, using galaxies from the five CANDELS/3D-*HST* fields ([Grogin et al. 2011](#); [Koekemoer et al. 2011](#); [Brammer et al. 2012](#)) to estimate a quenching timescale of 2–5 Gyr out to intermediate redshifts. They found that the quenching processes were fairly independent of the host mass, but were correlated with galaxy stellar masses and redshifts such that smaller galaxies at lower redshift have longer quenching time. These results, they argued, suggest that their galaxies stopped forming stars due to fuel (gas) depletion. In addition, their findings corroborate the *delayed-then-rapid* quenching scenario that [Wetzel et al. \(2013\)](#) found locally using SDSS, in which galaxies upon infall into a larger halo undergo a long delay phase where the satellite behaves indistinguishably from a central galaxy, and a short phase ($\lesssim 1$ Gyr) where the star formation rate drops below their detectability threshold.

These results outline a scenario where satellite galaxies retain their gas reservoirs for a substantial period of time after infall into a larger halo, but then rapidly lose both their gas and star formation. However, the gas depletion aspect of this is not directly measured, but rather inferred from the behaviour of the satellite population. The relative depletion times of the gas versus the star formation rate can provide insights into which physical processes are responsible. For instance, rapid removal of extended neutral gas while continuing star formation may indicate ram pressure stripping driving the quenching of satellites, while concurrent reductions in gas content and star formation may be more indicative of gas starvation. Upcoming observations of HI gas using telescopes such as the Square Kilometre Array (SKA) precursor MeerKAT will be able to test these scenarios directly. It is thus timely to theoretically investigate the co-evolution of gas and stars within haloes, both in order to test whether current models reproduce the observed behaviours, and also to make predictions for upcoming multi-wavelength observations.

Much work has previously been done on satellite quenching from the theoretical side. [McGee et al. \(2009\)](#) studied accretion history with a semi-analytic galaxy sample covering a wide range of environment, *i.e.* from groups to clusters. Their sample showed that cluster galaxies typically originate from smaller group galaxies, and as a consequence the environmental effect on the galaxies lasted > 2 Gyr. Their finding suggests that at $z > 1.5$, galaxies should experience at most mild environment processes. [Simha et al. \(2009\)](#) used an SPH cosmological simulation and found a decreasing but continuous gas accretion of the satellite galaxies. They showed that the gas depletion happens within $\sim 1 - 1.5$ Gyr timescale. These timescales were already longer than those typically assumed in semi-analytic models at that time, which ([Weinmann et al. 2006](#)) showed resulted in an overprediction of red satellite galaxies compared with observations.

[De Lucia et al. \(2012\)](#) used a semi-analytic galaxy formation model based on the Millennium Simulation to conclude that the majority of small galaxies are pre-processed satellite, *i.e.* they were previously located in smaller groups prior to their current one. By accounting for such an origin, their model predicted a relatively long timescale for satellite galaxies to lose their gas and halt their star formation (~ 6 Gyr). [Wetzel et al. \(2015\)](#) used high-resolution Local Group simulations from the Exploiting the Local Volume in Simulations (ELVIS) project, and found a rapid environmental

quenching timescale, shorter than $\lesssim 2$ Gyr for low-mass ($\sim 10^8 M_\odot$) satellite galaxies, with an additional 1–2 Gyr when including the pre-processing event. The quenching timescale positively correlates with the satellite stellar mass up to $\sim 10^9 M_\odot$ up to very large values of close to 10 Gyr, before decreasing for more massive satellites down to ~ 5 Gyr. Hence N-body plus semi-analytic models generally require a quite long quenching timescale in order to match observations. It is worth mentioning the Empirical Model for the foRmation of GalaxiEs (EMERGE, [Moster et al. 2018](#)) which uses the delayed-then-rapid quenching model to successfully fit the cosmic evolution of galaxy populations.

Our previous work in [Rafieferantsoa et al. \(2015\)](#) examined satellite quenching using cosmological entropy-conserving Smoothed Particle Hydrodynamics (SPH) simulations with a simple model for quenching massive galaxies via gas ejection. We found a halo mass dependent timescale, where galaxies in more massive structures lose their gas and shut off star formation faster than those living in less massive host: ~ 1 and ~ 2.5 Gyr *e*-folding times respectively. Qualitatively, this agrees with the semi-analytic model results, but overall the timescales are shorter. The range of predicted quenching times suggest that the timescales depend on a variety of factors, including physical ones such as halo mass and redshift, and perhaps numerical ones such as resolution and hydrodynamic methodology ([Agertz et al. 2007](#)). It would clearly be an improvement to use cosmologically-situated gas dynamical simulations at high resolution, including a more physically motivated quenching model with more accurate hydrodynamics.

In this paper, we aim to do this using galaxies from high-resolution cosmological zoom simulations of 2 galaxy groups with virial masses $> 10^{13} M_\odot$ using the GIZMO code that better handles surface instabilities ([Hopkins 2015](#)), and including a halo heating model for radio mode quenching ([Bower et al. 2006](#); [Croton et al. 2006](#); [Gabor & Davé 2015](#)). These zooms are extracted from the MUFASA cosmological simulation ([Davé et al. 2016](#)) and re-run with nearly identical feedback physics, but at 64 \times better mass resolution. We track satellites falling into the primary groups in order to directly quantify the duration from infall until when the galaxies lose their gas and stop forming stars. We quantify both the delay time when satellites still behave similar to centrals of the same mass, and the fading time over which satellites suddenly transition from being gas-rich and star-forming to gas-poor and quenched. The timescales for gas evacuation and quenching are comparable. The delay time is generally $\sim 1 - 2$ Gyr, and drops rapidly with the infall mass of the satellite, while decreasing modestly to higher redshifts. In all cases the fading time is much smaller than the delay time (typically $\lesssim 0.2$ Gyr), and it is somewhat longer for more massive infalling objects. Our quenching timescale thus follows a *delayed-then-rapid* scenario inferred from observations ([Wetzel et al. 2013](#)), showing that this is a natural consequence of the interplay between hydrodynamics and feedback physics within galaxy groups.

§2 briefly reviews the MUFASA simulation model used for this work, with the description of the method used to get our galaxy sample and find progenitors. In §3, we examine the distribution of galaxy properties used in this work, particularly gas content and star formation histories. In §4, we quantify the depletion timescale of HI and SFR while §5 and §6 show the relation between gas and SFR, and gas and halo mass, respectively. We summarize our findings in §7.

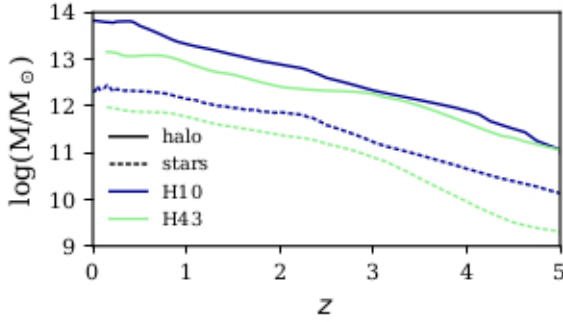


Figure 2. Total masses of the dark matter (full lines) and star (dashed lines) particles vs redshift z of H10 (dark blue) and H43 (light green) at the refined resolution.

2 SIMULATIONS

2.1 Galaxy formation model

To analyse the evolution of galaxy H I content, we use the MUFASA galaxy formation models fully described in [Davé et al. \(2016\)](#). The same model was used in [Rafieferantsoa & Davé \(2018\)](#) with minor differences. This section briefly describes the main prescriptions in MUFASA necessary for galaxy formation as well as the changes we made to fit the context of this work.

First is the star formation rate (SFR) prescription that is based on the molecular content of the gas particles. It follows a power law scaling, namely the [Schmidt \(1959\)](#) relation:

$$\text{SFR} = \epsilon \frac{\rho f_{\text{H}_2}}{t_{\text{d}}}, \quad (1)$$

where $\epsilon = 0.02$ is the star formation efficiency ([Kennicutt 1998](#)), f_{H_2} is the molecular hydrogen fraction in the gas volume element and t_{d} is the dynamical time of the gas with density ρ . The star formation prescription is only applied to gas particles above a number density threshold of $n_{\text{thresh}} = 0.13 \text{ cm}^{-3}$. Such high density is only reached when the gas particles undergo radiative cooling. MUFASA uses the GRACKLE 2.1 library¹ for cooling, which accounts for H/He-elements and metal-line cooling. During the simulation, a uniform background metagalactic radiation field is assumed following [Faucher-Giguère et al. \(2010\)](#).

Galactic winds driven by supernovae and young star radiation pressure are also accounted for in our model. Instead of modeling the detailed physics that is beyond our resolution capabilities, MUFASA uses scaling relations taken from the Feedback In Realistic Environment (FIRE, [Hopkins et al. 2014](#)) simulations analysed in [Muratov et al. \(2015\)](#) that model their combined effects into a mass outflow rate and velocity. The mass loading factor η and outflowing speed v_w are thus taken to be:

$$\eta = 3.55 \left(\frac{M_*}{10^{10} M_{\odot}} \right)^{-0.35} \quad \text{and} \quad v_w = 2v_c \left(\frac{v_c}{200 \text{ km s}^{-1}} \right)^{0.12}, \quad (2)$$

where M_* and v_c are the stellar mass and circular velocity of the galaxy which the gas volume element belongs to; we determine these quantities using an on-the-fly friends-of-friends galaxy finder, and

¹ <https://grackle.readthedocs.io/en/grackle-2.1/genindex.html>

get the circular velocity using the observed baryonic Tully-Fisher relation. To eject gas elements, we apply a velocity kick perpendicular to the local cross product of the velocity and acceleration.

To prevent the overproduction of stars in massive ellipticals, MUFASA uses a heuristic prescription based on the hot halo quenching scenario in [Gabor & Davé \(2015\)](#), which follows from semi-analytic work showing that “radio mode” quenching can yield a reasonable quenched galaxy population ([Bower et al. 2006](#); [Croton et al. 2006](#)). The idea is to stop further supply of gas inflow for galaxies within host haloes above a threshold quenching mass of $M_q > (0.96 + 0.48z) \times 10^{12} M_{\odot}$, which is taken from the analytic equilibrium model of [Mitra et al. \(2015\)](#). In MUFASA this is done by heating all the gas to the virial temperature $T_{\text{vir}} = 9.52 \times 10^7 M_h^{2/3}$ ([Voit 2005](#)) of the haloes, excluding gas that is self-shielded, i.e. has an H I fraction above 1% after the self-shielding prescription of [Rahmati et al. \(2013\)](#) is applied. One significant difference with respect to the implementation in MUFASA is that we only heat the gas particles within the inner 25% of the virial radius of the haloes, rather than the entire halo, in order to mitigate the overproduction of quenched satellite galaxies as found in [Rafieferantsoa & Davé \(2018\)](#).

2.2 Zoom simulations

The cosmological parameters values used in this work are $\Omega_m = 0.3$, $\Omega_{\Lambda} = 0.7$, $\Omega_b = 0.048$, $H_0 = 68 \text{ km s}^{-1} \text{ Mpc}^{-1}$, $\sigma_8 = 0.82$ and $n_s = 0.97$, consistent with [Planck et al. \(2016\)](#). Our parent simulation is a $50h^{-1} \text{ Mpc}$ on a side with 512^3 , with dark matter particles only, having identical random seeds to the $50h^{-1} \text{ Mpc}$ MUFASA simulation in [Davé et al. \(2016\)](#). The simulation starts at $z = 249$ with initial condition generated using Music ([Hahn & Abel 2011](#)). Once at $z = 0$, the haloes are identified using the friends-of-friends algorithm with a linking length of 2% of the mean inter-particle distance.

We apply the zoom-in technique for two carefully chosen haloes within our parent box, in which we re-simulate these haloes with all physical models at significantly higher resolution. To investigate the quenching of satellite galaxies, we focus on the mass range found in [Rafieferantsoa & Davé \(2018\)](#) where satellite quenching effects were most evident, namely $M_h \sim 10^{13} M_{\odot}$. Hence we select halo 10 (H10, hereafter) and halo 43 (H43, hereafter), having $z = 0$ masses of $5.5 \times 10^{13} M_{\odot}$ and $1.7 \times 10^{13} M_{\odot}$ at coarse resolutions. This is well above our quenching mass scale $M_q \sim 10^{12} M_{\odot}$, but nonetheless we find that the smaller halo has a central galaxy that is still star forming, owing to remaining cold gas in the halo and infall of gas-rich satellites. The larger halo has a quenched central. Our choice of haloes is further based on their evolutionary growth history, namely that these haloes did not have any major fly-by or merger during their evolution. This is to ensure that the haloes are evolved in a self-contained way and did not change their physical properties by interacting with other structures of similar size.

Our two haloes are re-simulated with dark matter particles 64 times lower mass than those from the primary box within the zoom region, plus a surrounding region with $8\times$ better resolution. The $64\times$ refined dark matter particles are further split into gas volume elements and dark matter particles based on our adopted baryon fraction (see §2.2). When resimulating, the center of mass of the highly resolved particles is shifted to the centre of the cubical low-resolution volume. Properties of the haloes presented in this work are summarized in Table 1. At the refined resolution, the H10 actually becomes slightly larger than in at the parent resolution, up to

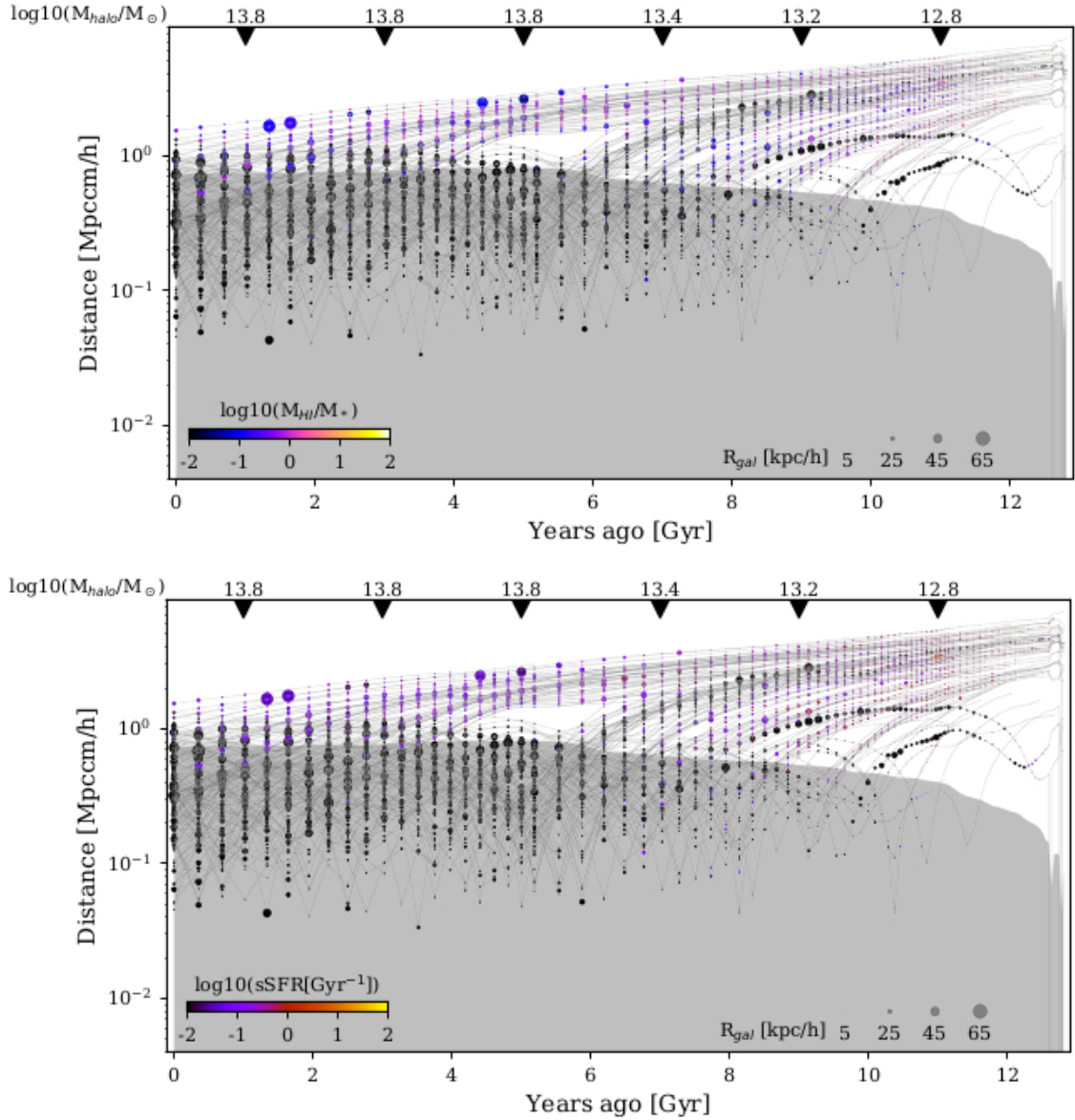


Figure 3. H I (top) and SFR (bottom) evolution of galaxies in the H10 zoom run. Each line shows the path of a galaxy relative to its distance to the center of main halo. The galaxies shown here are the galaxy members of the main halo at $z = 0$. The shaded area is the region inside the virial radii of the host. The evolution of the mass of the host is shown on the top of the panel.

Table 1. Zoom simulated haloes.

Name	Original $M_{\text{halo}} (M_{\odot})$	Refined $M_{\text{halo}} (M_{\odot})$	SFR _{central} (M_{\odot}/yr)	# of satellites	$M_{*,\text{central}}/M_{\text{halo}}$
H10 ($z = 0$)	5.578×10^{13}	6.625×10^{13}	0	182	0.02441
H43 ($z = 0.15$)	1.463×10^{13}	1.422×10^{13}	96.634	20	0.05538

$6.625 \times 10^{13} M_{\odot}$ ($z = 0$), while H43 drops slightly to $1.422 \times 10^{13} M_{\odot}$ ($z = 0.15$). The former has no central star formation, while the latter is forming stars vigorously at $\sim 100 M_{\odot}/\text{yr}$. The former also has far more satellites, 180 vs. 20, and hence the statistics of satellites in this paper is dominated by this larger H10 halo.

For illustration, Figure 1 shows H10 at $z = 0, 0.5, 2$ (top to bottom), with the left column showing the projected gas temperature,

the middle column showing H I column density, and the right column showing the stellar mass surface density. The circles indicate the sphere enclosing $200 \times$ the critical density at those epochs. At $z = 2$ (10 Gyr ago) it is evident that H I is distributed with the stars throughout the halo, and even shows some diffuse features outside of galaxies. By $z = 0.5$ (5 Gyr ago) there is a clearer segregation of H I towards the outskirts of the halo, though there remain some H I-rich

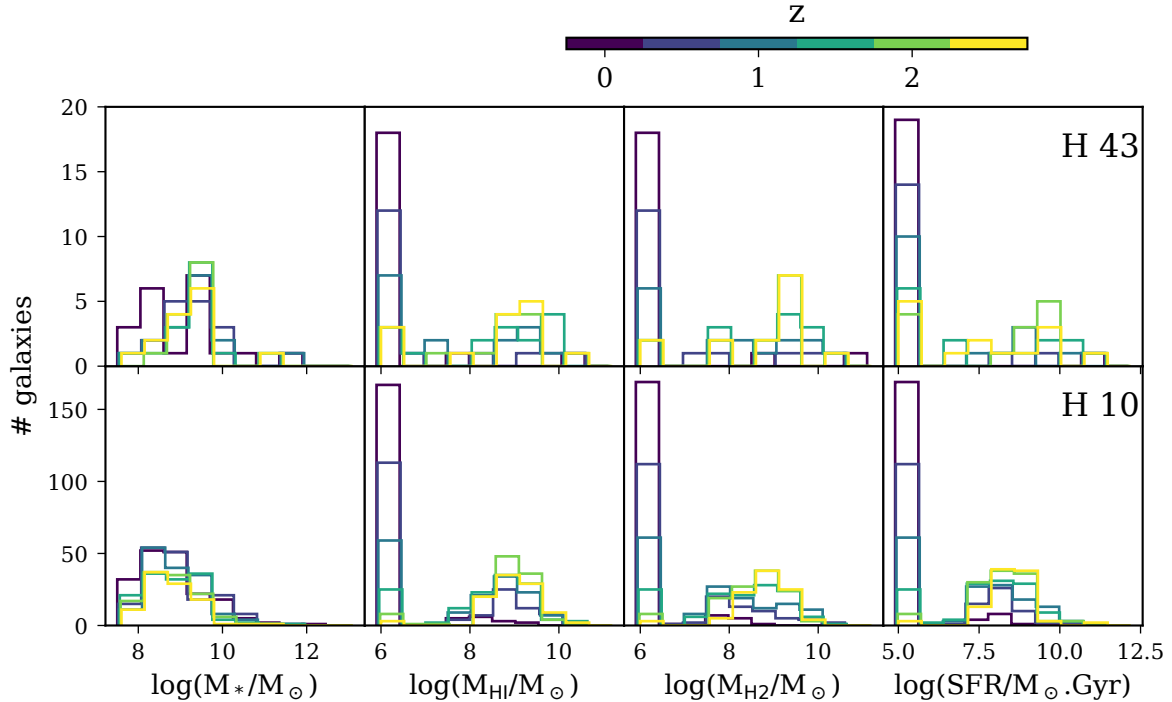


Figure 4. Evolution of the galaxy property distributions of our selected haloes. *Upper* panels are for H43 and *lower* panels for H10. Different colors represent the distributions at different redshift. Each column shows distributions for different galaxy properties.

galaxies within the halo. By $z = 0$, very little HI is left in the halo, as the hot $\sim 10^7$ K gas has grown to encompass the halo and beyond. This visually demonstrates the strong impact that environment and halo quenching have on the gas content of satellites.

Figure 2 illustrates the growth history in the total dark matter (full lines) and stellar (dashed lines) components in the H10 (dark blue) and H43 (light green) high resolution runs. These show that the haloes masses grow roughly in concert as expected (solid lines), but that the stellar mass (dashed lines) of the smaller halo grows more slowly until $z \sim 3$, and more rapidly at later epochs. In the end, the total stellar to halo mass ratio for the small group ends up significantly larger. These two haloes thus span the interesting mass regime where the smaller one is significantly retarded by star formation feedback at early epochs, while the more massive has an early-weighted growth history more typical of quenched massive galaxies today. These growth histories may help explain why H10 is fully quenched today, but H43 remains star-forming. One way to look at this would be to show the baryon conversion efficiencies but we leave such investigation of growth rates for future work, with larger samples.

Similar to other MUFASA papers, we use SKID² galaxy finder and the properties of galaxies and haloes are obtained from CAESAR³, which uses the yt simulation analysis suite as a backend. See Rafieferantsoa & Davé (2018) for details on the calculation of those properties including M_{halo} , M_* , M_{HI} , M_{H_2} and SFR of the galaxies.

3 EVOLUTION OF GAS AND STELLAR PROPERTIES

In this work we are primarily interested in the gas content and star formation history of the galaxies in our host haloes. Figure 4 shows the distributions of stellar mass (*left* column), the HI mass (2nd column), the H₂ mass (3rd column) and the star formation rate (*right* column) of the galaxies in H10 (*lower* panels) and in H43 (*upper* panels). The different coloured curves show the evolution from $z \approx 3 \rightarrow 0$ (yellow to violet). Galaxies are given lower-limit values once their HI, H₂, or SFR goes below the x-axis limit of our figure.

In the M_* panel, one sees a buildup of smaller accreted satellites within the halo as time passes, while the most massive galaxy grows steadily in time. The gas content is higher at intermediate redshifts, and then the population of gas-free satellites builds up at low redshifts. There is a lot of similarity in the HI, H₂, and SFR distributions, showing that these quantities seem to broadly evolve together, even within a galaxy halo. The H43 halo (*lower* row) shows qualitatively similar trends, though the galaxies themselves tend to be less massive, and there are many fewer satellites (note the y-axis scale). Given these distributions of galaxy properties in our haloes, we can look at the evolution of HI and H₂ content and their timescales for consumption.

With our simulated outputs spaced by ~ 300 Myr at $z \sim 0$ and shorter intervals at higher redshift, we can track individual galaxies based on their stellar masses. We match the galaxies between two successive snapshots and identify the galaxies with the maximum number of similar star particles. An issue with this method is that the progenitor of a smaller galaxy flying by a bigger galaxy would have its progenitor always then be the bigger galaxy. To avoid this, we further match the galaxies between snapshots at two separated time intervals, in order to avoid mischaracterising fly-bys as mergers.

² <http://www-hpcc.astro.washington.edu/tools/skid.html>

³ <https://bitbucket.org/laskalam/caesar>

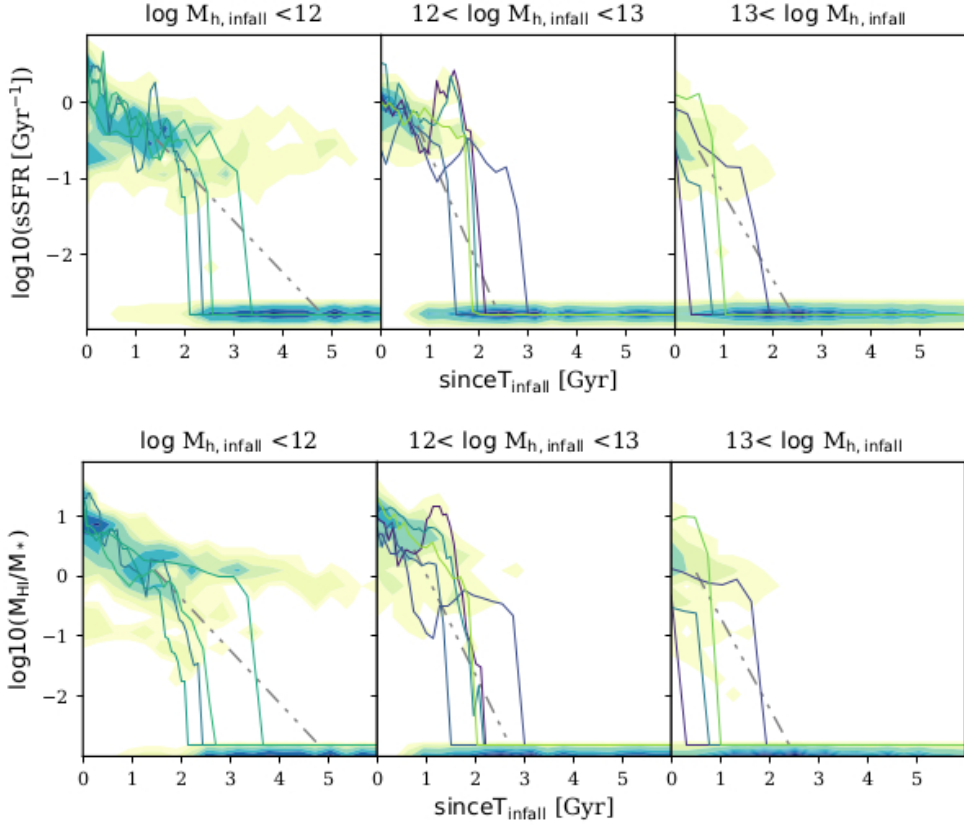


Figure 5. Specific star formation rate (*upper panels*) and HI-richness (*lower panels*) of galaxies since they became satellite. The mass ranges of the halo at infall ($M_{h,infall}$) are shown on top of the panels. Note that all the galaxies belong to H10 at $z = 0$. It is clear that galaxies still form stars for ≥ 5 Gyr when $M_{h,infall} \leq 10^{12} M_{\odot}$. That time decreases down to ~ 1 Gyr for $M_{h,infall} > 10^{13} M_{\odot}$. The gray dashed lines connect the median values of the upper and lower contours. The lines show tracks of representative galaxies in each $M_{h,infall}$ range.

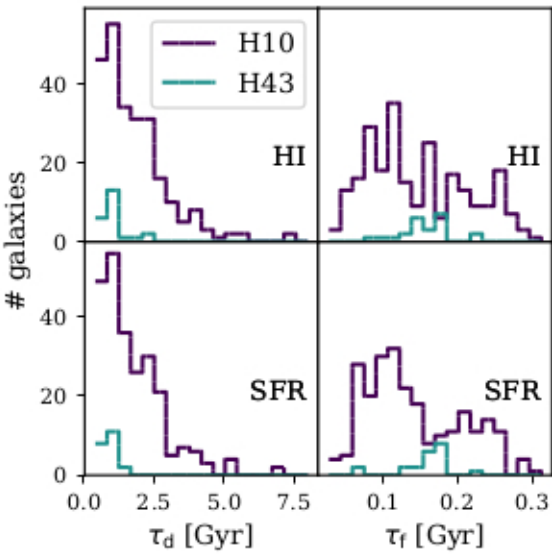


Figure 6. Delay time (*left panels*) and fading time (*right panels*) distributions of the galaxies at $z \leq 1$ quantified by the SFR (*lower panels*) and the HI content (*upper panels*). Purple lines for H10 and blue lines for H43

Figure 3 shows the distances to the progenitors of galaxies present in the host halo (H10) at $z = 0$. The size of the circles show the total baryonic mass of the galaxy (gas+stars), and the colour of the circles show the properties of the galaxies as indicated in the colour bar – HI in the top panel, and SFR in the bottom panel. The shaded region represents R_{200} at any given epoch. The groups build up hierarchically. In this work, we are only concerned about the progenitors of the galaxies present in the main halo at $z = 0$. We can clearly see that when galaxies cross the virial radius of the halo of interest, their HI-richness (or sSFR) is considerably depleted and the only growth of galaxies is via dry mergers (*e.g. Oser et al. 2010*). The following sections try to quantify the timescale required for such events. Throughout this work, we use H10 and H43 data except for the latest redshift where we only use H10 because H43 was stopped at $z \geq 0.15$.

4 SATELLITE QUENCHING TIMESCALES

Cold gas within galaxies is diminished because of environmental effects within the virialised regions such as stripping (ram pressure and tidal) and the lack of gas inflow (or starvation), along with the consumption of gas in the interstellar medium via star formation and outflows. Estimated observed timescales for quenching are t_q of 5 – 7 Gyr (*Wetzel et al. 2013*) or 1 – 2 Gyr (*Oman & Hudson 2016*), depending on the galaxy masses and the environment they live in: the more massive the galaxies or the haloes, the shorter

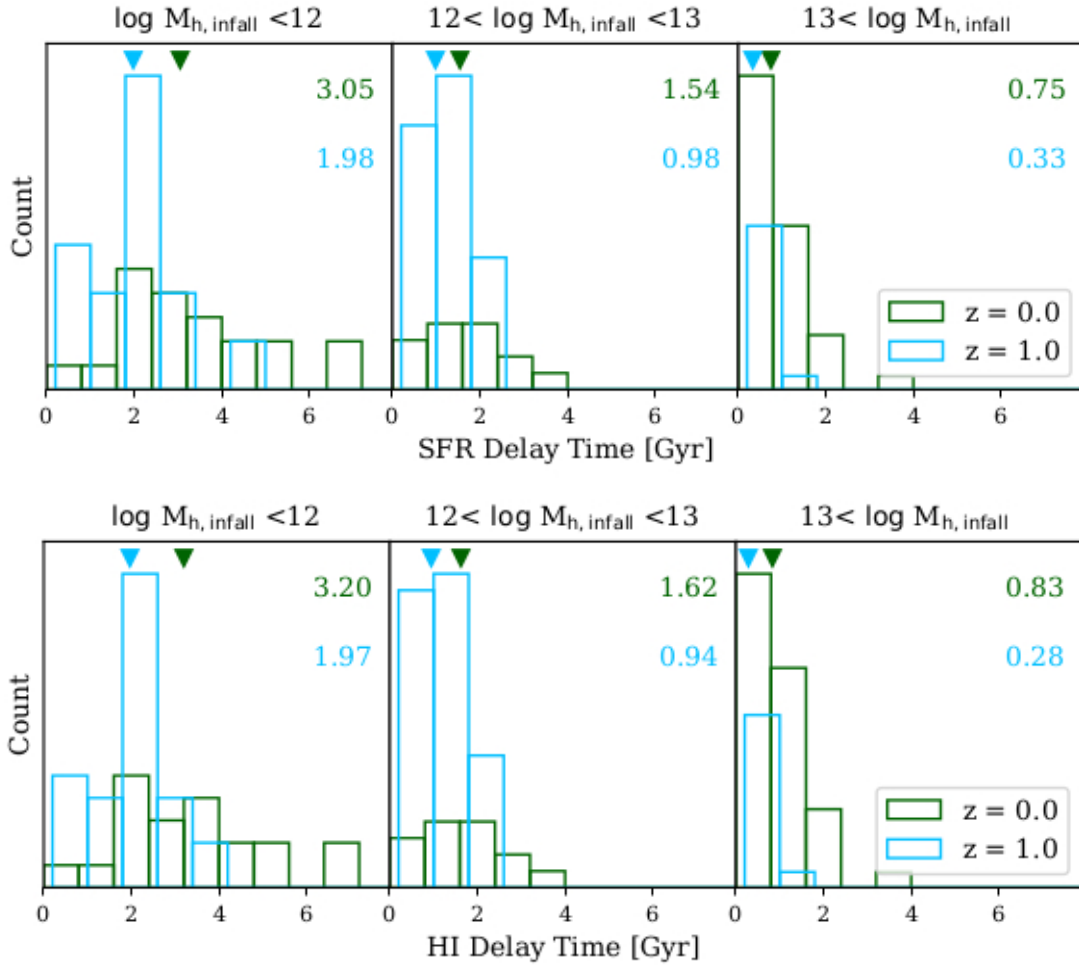


Figure 7. *Upper (Lower)* panels show the sSFR (HI-richness) delay time distributions. *Left* panels are for the galaxies first falling in $\log M_{h, \text{infall}} < 12$, the *Middle* panels for $12 < \log M_{h, \text{infall}} < 13$ and the *Right* panels for $13 < \log M_{h, \text{infall}}$. The downwards triangles on the top of the panels point to the mean values of the delay times where the corresponding values are shown on the top right (color coded).

the timescales. Here we quantify these timescales using our zoom simulations to emphasise on the differences between the gradual starvation of the galaxies by lack of inflowing cold gas, and the rapid drop of star formation rate due to the remaining molecular content being used up.

We define the starting time t_0 of the gas depletion and star formation quenching to be when a galaxy falls into a more massive halo and becomes satellite. We only include galaxies that were always central prior to t_0 . Fossati et al. (2017) used the same definition of t_0 , and they found a 2-5 Gyr timescale for quenching the satellites. They found that the fraction of quenched satellites is higher at lower redshift and higher halo masses. Surprisingly, they found no dependence of the passive central galaxy fraction with halo masses (see their fig. 17).

Figure 5 shows the 2D distributions in time after t_0 versus the sSFR (top panel) and the HI fraction (bottom) for satellites in H10. The left panels are for galaxies falling in primaries with $M_{\text{halo}} < 10^{12} M_{\odot}$, the middle panels show $10^{12} M_{\odot} < M_{\text{halo}} < 10^{13} M_{\odot}$, and the right panels show $M_{\text{halo}} > 10^{13} M_{\odot}$. The dashed lines go from the median values of the upper contours to the median values of the lower contours.

We define the quenching timescales (t_q) to be the time

since t_0 when the galaxy last reaches $\text{sSFR}_{\text{lim}} < 10^{-2}$, or $\text{sSFR}_{\text{lim}} < 10^{-2} \text{ Gyr}^{-1}$; thus we have a gas quenching timescale and a SFR quenching timescale. The dashed lines in Figure 5 suggest a shorter t_q for higher infall halo masses. This is in contrast to Fossati et al. (2017) who did not find any such dependence in their observed sample. We speculate this to originate from the difference between the simulated and observed galaxy properties. For instance, the halo mass of the simulated galaxies are computed using the friends-of-friends technique directly on the 3D-position of the galaxies, whereas a matching technique between observed and mock galaxies is used for the 3D-HST sample in Fossati et al. (2017). The uncertainty in redshift space of ± 0.1 between the observed galaxies and the the mock catalogue might impact their finding on the environment dependence of the quenching timescale. In addition, the stellar mass threshold of their sample becomes as high as $> 10^{10} M_{\odot}$ for $z > 1$, affecting the galaxy number density and the matching technique thereafter.

4.1 Computing delayed-then-rapid quenching

We further split t_q into a *Delay Time* τ_d during which the satellite properties are similar to a central galaxy of the same mass, and

a *Fading Time* τ_f during which strong depletion happens and the H α -richness or sSFR reaches the threshold limit. We note that those definitions are similar to those used in Fossati et al. (2017).

We compute τ_d in our simulations as the time between t_0 and the earliest snapshot before the instantaneous rapid drop of sSFR or H α richness occurred. τ_f is then the remainder of the time to quench ($t_q = \tau_d + \tau_f$), i.e. the duration from the beginning of the rapid drop to the next time the quantity is below the threshold. The fading time typically happens within two successive snapshots in our simulation, that is, on timescales less than a couple hundred Myr. In that case we interpolate the value based on an exponential fit, but these numbers may be uncertain.

For $z \leq 1$, we show in Figure 6 the histograms of the delay time and the fading time for satellites in H10 (purple) and H43 (blue). The distributions of the delay times (left panels) show similar trends between the two haloes, indicating a power law distribution of delay times. In contrast, the fading times (right panels) are less similar, *i.e.* τ_f from H10 tend to show double peak distributions whereas those from H43 with only single peaks. The difference is less conclusive due the very small number of galaxies in H43.

4.2 Delay Time

Most of the quenching time is spent in the delay phase where satellite galaxies evolve similarly to central galaxies. Wetzel et al. (2013) and Fossati et al. (2017) found $\tau_d > 80\%$ the total quenching time. Figure 7 shows the distribution of delay times for the sSFR (upper) and the H α fraction (lower) of galaxies. The downward triangles at the top of the panels show the mean values of the delay times at different redshift: $z = 0$ (dark green), $z = 1$ (light blue). Left to right panels show the results for increasing halo mass at first infall. The distributions span a wide range of values especially for $z = 0$. The mean values differences between the two different redshift are higher for lower halo mass at first infall. The different timescales at different epochs hint a star formation efficiency difference that we will explore in §5 and §6. SFR and H α delay times show similar trend in their distributions.

To further analyse these trends, we also bin our data based on the galaxy stellar masses and look at the evolution of the delay timescales at different redshift. Figure 8 shows the sSFR and H α -richness mean delay times τ_d : *upper* and *lower* panels respectively. *Left* to *right* panels show the results for increasing halo masses within which the galaxies first fall in. Each panel is divided into 6 sections: two columns for binned stellar masses of the infalling galaxies at t_0 (*left*: $M_{*,\text{infall}} < 10^9 M_\odot$ and *right*: $M_{*,\text{infall}} \geq 10^9 M_\odot$) and three rows for different redshift (*upper* for $z = 0$, *mid* for $z = 0.5$ and *lower* for $z = 1$). The numbers on the figure show the average τ_d . We note that at higher redshift, we only track the galaxies present in the main halo progenitors at that redshift, *i.e.* we do not include the progenitors of galaxies that are present in the $z = 0$ main halo but did not cross the virial radius by that given redshift.

The mean of the delay times is the longest for the least massive host halo at $z = 0$ (~ 3 Gyr), and decreases down to ~ 1 Gyr by $z \sim 1$. The galaxies falling in the most massive halo of infall take the shortest delay time: ~ 1.5 Gyr faster than those falling in $M_{h,\text{infall}} \leq 10^{12} M_\odot$ (*i.e.* ≤ 1 Gyr). Less massive satellite galaxies have longer delay time (1 Gyr more) than their massive counterparts, except for those falling in the most massive structure where this scenario is flipped. H α -richness and sSFR delay times show similar behaviour, which we explore in more detail later.

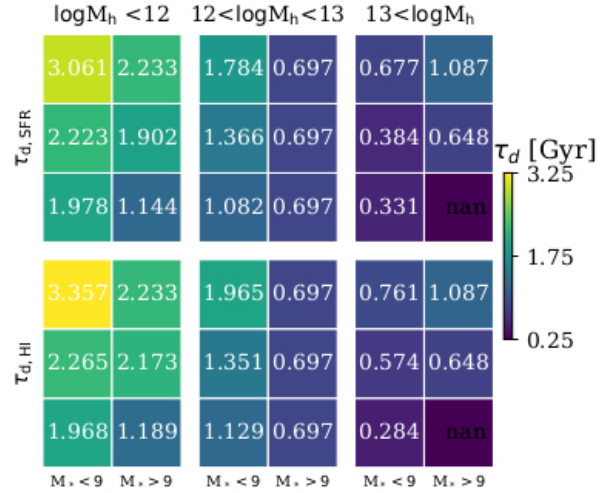


Figure 8. Delay time τ_d for sSFR (*upper* panels) and H α -richness (*lower* panels). *Left* panels are for galaxies becoming satellite in $M_{h,\text{infall}} < 10^{12} M_\odot$, *center* panels for $10^{12} \leq M_{h,\text{infall}} < 10^{13} M_\odot$ and *right* panels for $10^{13} M_\odot \leq M_{h,\text{infall}}$. Each panel is further divided into 6 areas: 2 columns for stellar mass bins at infall ($M_{*,\text{infall}} < 10^9 M_\odot$ *left* and $M_{*,\text{infall}} \geq 10^9 M_\odot$ *right*) and 3 rows for different redshifts (*upper* for $z = 0$, *middle* for $z = 0.5$ and *lower* for $z = 1$). See Figure 7 for the distribution of galaxies in terms of τ_d .

4.3 Fading Time

In the delayed-then-rapid scenario, the fading time τ_f is expected to be much shorter than the delay time. Fossati et al. (2017) computed the delay time by matching the star formation efficiency, quantified by the main sequence parameterisation of Wisnioski et al. (2015), between the 3D-HST sample and their mock catalogue. They estimated $\tau_f = t_q - \tau_d < 0.6$ Gyr.

Similar to §4.2, we also look at the timescale distributions as shown in Figure 9. In this case, the mean values (downward triangles) do not show clear patterns with halo mass at first infall. With respect to time, we can see that the longer timescale at lower redshift is still present. Keep in mind that owing to the small values for τ_f and the spacing of our simulation snapshots, the values are less precise and some trends may be washed out.

Figure 10 shows the mean fading times τ_f of the H α -richness (*lower* panels) and sSFR (*upper* panels). All scenarios show mean fading time of ~ 50 – 200 Myr. Generally, lower redshift (*upper* parts of each panel) infall requires longer τ_f to suppress the star formation and the neutral gas content compared to their counterparts at higher redshift (*lower* parts of each panel). Interestingly, galaxies falling into the most massive host tend to require more time to completely consume their gas and stop star formation, e.g. ~ 185 Gyr for sSFR and ~ 200 Myr for H α -richness for galaxies at $z = 0$, which might be due to our limited sample and requires further analysis. The stellar mass of the galaxies does not show any trend in the fading time, *i.e.* difference between the *left* and *right* areas in each panel.

In summary, the delay time τ_d is typically in the range of ~ 1 – 3 Gyr, longer for lower stellar and halo masses until the haloes exceed $10^{13} M_\odot$. In the latter case, less massive galaxies have τ_d of ~ 400 Myr lower than more massive ones. Galaxies have longer τ_d when they become satellite more recently. The numbers are very similar for both H α and sSFR, which suggests that the SFR is being attenuated owing to the removal (or stripping) of the extended gas reservoir. The fading time τ_f , in contrast, is always very short, and

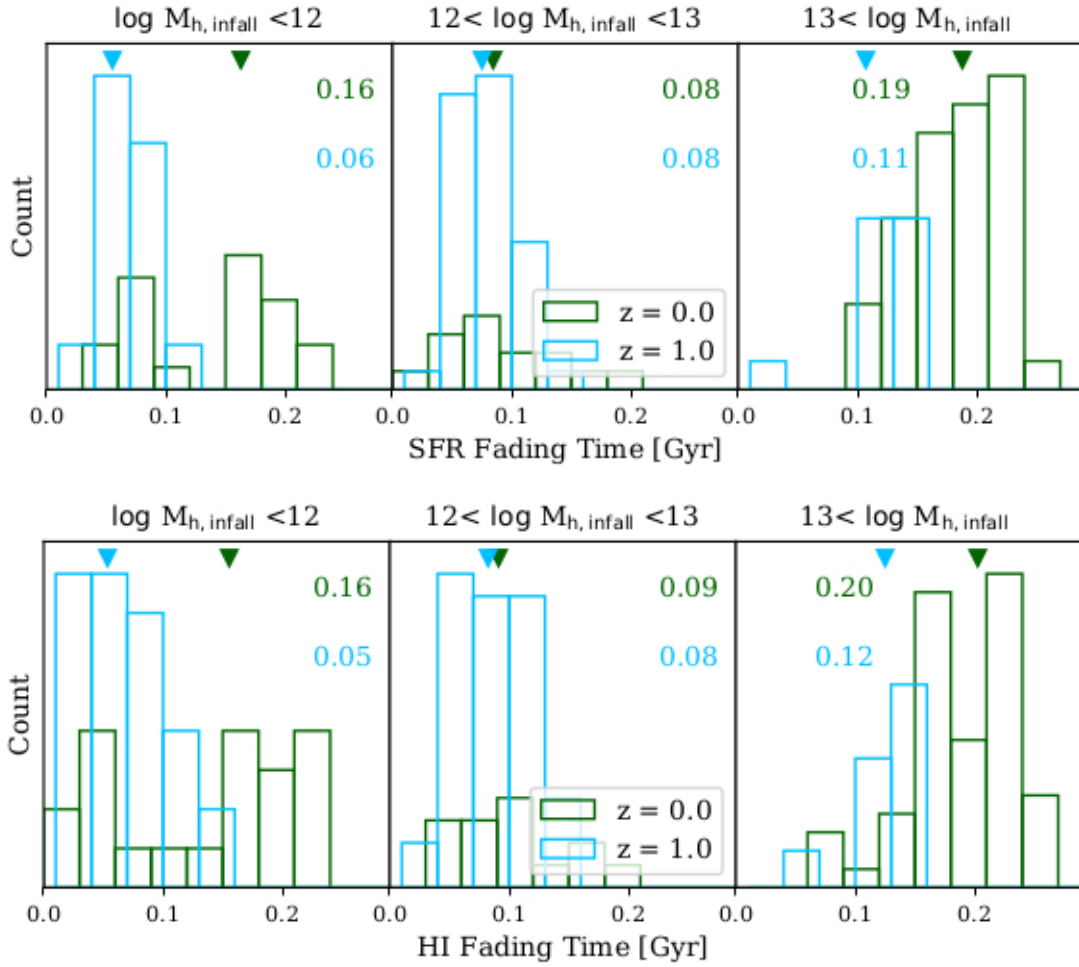


Figure 9. Similar to Figure 7 but showing for the Fading Time τ_f .

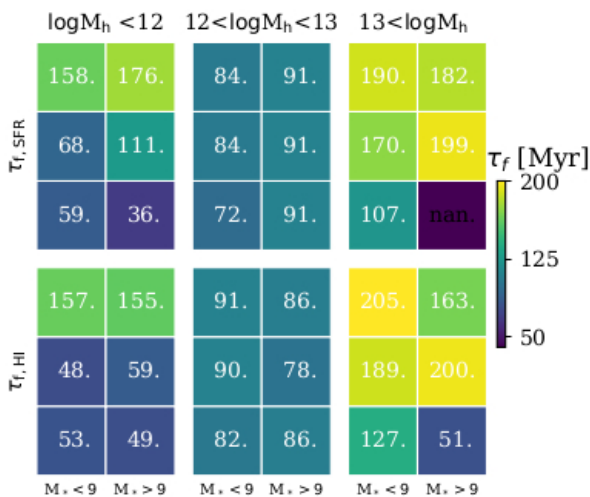


Figure 10. Similar to Figure 8 but showing for the Fading time τ_f binned by stellar mass.

shows the opposite trends. Generally, galaxies falling into higher halo masses have longer τ_f . The case is less clear at $z = 0$ but

becomes more apparent at higher redshift. The difference for lower and higher galaxy stellar masses is minor if nonexistent.

At face value, we find similar trends to [Fossati et al. \(2017\)](#) in terms of stellar mass, but our timescale dependence with halo mass was not seen in their 3D-HST sample, and our delay times are generally shorter by a factor of two or so. Assessing the significance of these discrepancies likely requires performing a more careful comparison where we create a mock sample with grism data and photometry and select and analyse this in the same way; we leave this for future work. For now, we note that the broadly similar trends as seen in observations both locally and intermediate redshifts are encouraging, and we predict for future H α surveys that the delay and fading times should be similar for the gas and SFR, at least in this halo mass range.

5 RELATION BETWEEN GAS CONTENT AND STAR FORMATION

The cooling and coalescence of neutral hydrogen into dense molecular clouds are important steps before the star formation. However, the formation of stars can disrupt the collapse of cold gas and therefore reduce later star formation. To better understand the driver

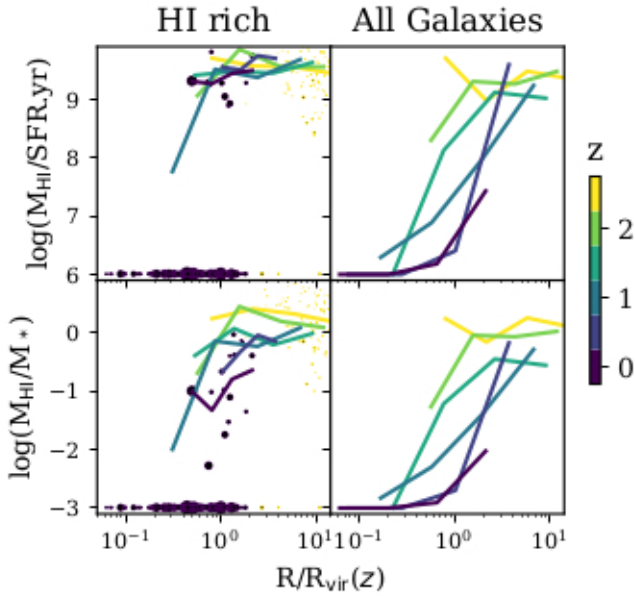


Figure 11. HI-consumption time (*upper panels*, $\log(M_{\text{HI}}/\text{SFR})$) and HI richness (*lower panels*) of galaxies vs their radial distances from the center of the host halo. The circles show the galaxies at the lowest (purple) and highest (yellow) redshift presented here. The lines show the mean values, colour coded by the redshift. Higher redshift galaxies are the progenitors of the low redshift galaxies. The low redshift galaxies are only the members of the main halo. Galaxy properties below 6 (for HI-consumption time) and -3 (for HI-richness) are given those lower limit values to confine the figure. *Left panels* show the mean values for only gas rich galaxies but *Right panels* show the mean values for all galaxies.

of satellite quenching, here we quantify the star formation activity given the amount of cold atomic and molecular gas.

Left panels of Figure 11 show the evolution of HI-richness (*lower panel*) and HI-consumption time (M_{HI}/SFR , *upper panel*) with respect to their distance to the main and its progenitors center of masses. Note that we only follow all the progenitors of the galaxies present in the $z = 0$ main halo. The purple dots are the galaxies at $z = 0$, with the purple lines showing the mean values. Yellow dots are the progenitors of the $z = 0$ galaxies at $z = 2.5$, with the yellow lines the mean values. Lines with different colors are the mean values at different redshift as shown in the colorbar. We did not show the galaxies themselves to avoid cluttering of the figures. Galaxies without cold gas are shown at the bottom of each panel but are not included in the calculation of the mean quantities. This is because we are only interested in those that still have HI. The virial radii used in the x-axes is for the progenitors of the main halo not for the individual galaxies.

A first look, the *left panels* of Figure 11 indicates that our galaxy sample has higher gas content at higher redshift, the galaxies lose their gas until today (*lower panel*), and those crossing the virial radius contain less HI. The HI-consumption time (*upper panel*) is barely a function of redshift and distance to the center of the main halo progenitors. This reinforces the idea of gas consumption via star formation, and the quenching of the latter by depletion of the former. This scenario remains the same at different cosmic times. We speculate that the dichotomy present in HI-consumption time being analogous to that in HI-richness indicates the existence of an HI-richness threshold below which further star formation is unlikely

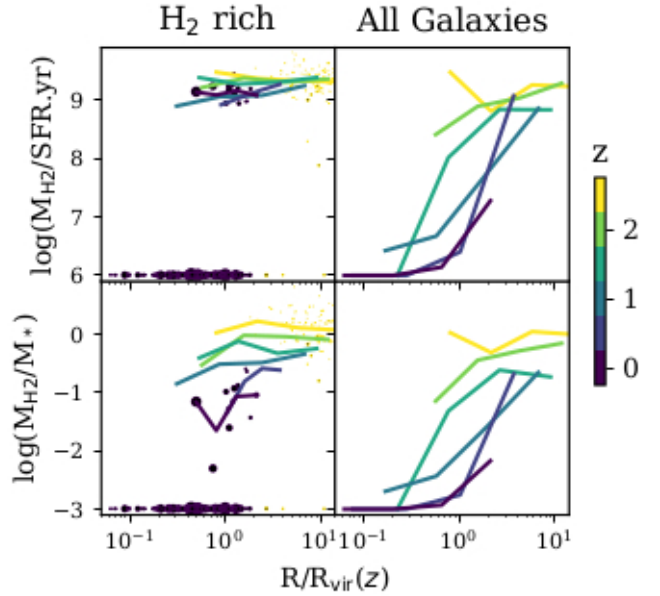


Figure 12. Similar to Figure 11 except showing for H₂ content.

to happen without any extra supply of cold gas and above which the star formation rate correlates directly with the HI content, even though the star formation is actually occurring within the H₂ gas.

Left panels of Figure 12 show the H₂-richness and H₂-consumption time to further analyse the gas consumption. The relationship is cleaner compared to the previous one, mainly due to our star formation prescription scaling with the H₂ fraction (f_{H_2} , see equation 1). Again, the pattern shows that galaxies contain less gas in molecular form at lower redshift than at higher redshift (*lower panel*) and their star formation rate proportionally declines with it (*upper panel*), *i.e.* unchanged H₂-consumption time at different radial distance and different redshift. The similarity between the HI-consumption time and the H₂-consumption time suggests the HI to be a direct tracer of star formation rate above a certain mass threshold. To test this, we can increase our group sample and vary the gas element density thresholds for self-shielding and star formation. We plan to investigate on this in future work.

Statistically, we can do the same exercise but including all the galaxies regardless of their gas content. In this case, we are looking at the general trend rather than the process towards being quenched as we argued previously. *Right panels* of Figures 11 and 12 are similar to the left, except that we now show the mean values for all the galaxies. The trend remains the same at the highest redshift, but the growth of no-cold-gas galaxies at lower redshift shifted down the mean values.

In short, the gas consumption timescale is neither a function of the group-centric distance nor the cosmic time. This is seen in both atomic and molecular hydrogen contents of the galaxies suggesting that above a certain mass threshold, HI alone can be a direct indicator of star formation. We note that our star formation prescription directly ties the H₂ content to star formation rate, while there is likely to be a more stochastic correlation that is sensitive to local interstellar medium conditions which are unresolvable in our cosmological simulations (Hu et al. 2016; Naab & Ostriker 2017). Hence the tightness of H₂ and SFR may be partly an artifact of our

star formation prescription, but the tightness with the H I and SFR is unlikely to be significantly impacted by this

6 RELATION BETWEEN GAS CONTENT AND HALO MASS AT INFALL

We showed previously that satellite galaxies have shorter delay times when they fall into more massive hosts. In that vein, we look at the change of gas-richness and gas-consumption time depending on the first halo of infall in this section.

Figure 13 shows the gas-richness (*lower panels*) and gas-consumption time (*upper panels*) of galaxies vs the mass of the haloes they fall in. The left panels show for H I content whereas the right panels for H₂ content. Generally, the decrease of H I-richness is faster when it falls in more massive haloes (*lower panel*) similar to what was found in Rafieferantsoa et al. (2015). However, such attributes are only true at lower redshift (purple, $z \sim 0$) but is not seen at the higher redshift explored here (yellow, $z \sim 1$). The *upper* panel shows that galaxies form star less efficiently early on for a given halo mass of infall: *i.e.* yellow > green > blue. The trend is very robust at higher halo mass of infall while at lower host halo masses, the trend becomes less coherent. This is due to the decreasing number of galaxies above our H I richness threshold at later time as infall in less massive host mostly happened earlier than infall in more massive ones. The H I-consumption time is independent of halo mass at infall at higher redshift but anti-correlates strongly at lower redshift.

In terms of molecular content, H₂-richness is less of a function of halo mass of infall than H I-richness and the correlation is barely present if not missing at any $z \leq 1$. H₂-richness at high halo mass of infall is higher at higher redshift, while it is less conclusive at the lowest masses. H₂-consumption time is flat with respect to the halo mass of infall. We barely see any evidence of consumption time difference at different redshift that was relatively apparent with H I-consumption time at higher halo mass of infall.

7 CONCLUSION

We use two zoomed-in groups of galaxies to study the timescales at which the H I content and the sSFR deplete when the galaxies become satellite. We determine the timescale for quenching t_q , and use observationally-motivated definitions to partition this into a delay time τ_d during which there is a gradual drop in star formation rate and gas content, and a fading time τ_f when the galaxy becomes quenched. We compare the results for τ_d and τ_f for star formation quenching, and for H I removal. We also quantify the efficiency of gas to form stars as well as the evolution of gas content depending on the halo mass of infall. We summarize our finding as follows:

- The delay times are in the range of $\tau_d \sim 0.3 - 3$ Gyr, while the fading times are much shorter ($\tau_f \sim 50 - 200$ Myr). This shows that these simulations are consistent with a delayed-then-rapid quenching scenario for satellites in group-sized haloes.
- Halo mass at infall ($M_{h, \text{infall}}$) has a strong effect on the delay time. Low- $M_{h, \text{infall}}$ haloes have large τ_d , while high- $M_{h, \text{infall}}$ haloes have $\tau_d \ll 1$ Gyr. τ_d also evolves with redshift, such that they are shorter at $z = 1$ than $z = 0$. Finally, galaxies with higher M_* for a given $M_{h, \text{infall}}$ tend to have shorter τ_d , except for the most massive $M_{h, \text{infall}} > 10^{13} M_\odot$ for which the trend is reversed.
- For the fading time, all values are quite small – ranging between 50 and 200 Myr – and typically less than the spacing between

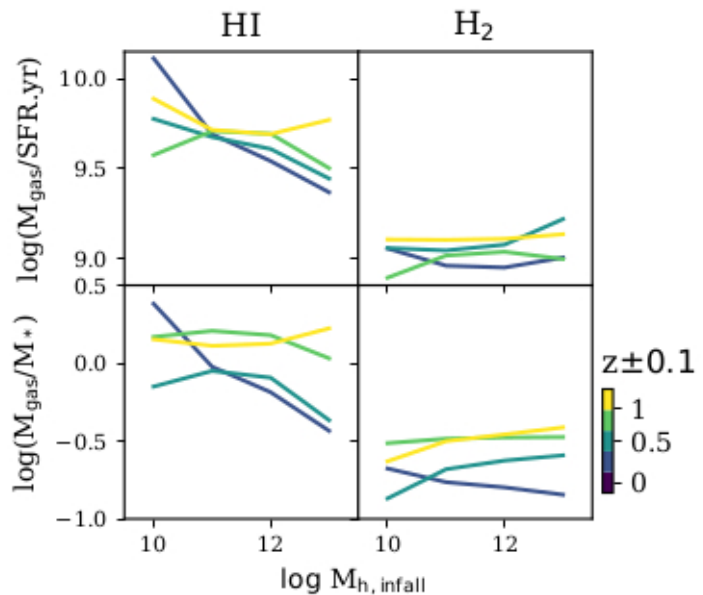


Figure 13. Gas-consumption time (*Upper*) and gas-fraction (*Lower*) of galaxies vs the halo mass they first fall in. *Left (Right)* panels are for H I (H₂). We use a binwidth of 0.2 around the redshift values (hence the $z \pm 0.1$ on the colorbar).

individual snapshots, so they are somewhat uncertain. There are no clear trends, except perhaps that τ_f seems to be slightly longer at high $M_{h, \text{infall}}$.

- The delay times for star formation quenching and H I removal are remarkably similar, and show the same trends as a function of $M_{h, \text{infall}}$ and M_* . This suggests that the H I gas is being depleted in concert with the star formation being quenched, broadly indicative of starvation-like mechanisms being the dominant driver during the delay phase. Meanwhile, the rapid fading time in all cases suggests that ram pressure stripping dominates this final quenching phase, but we lack the time resolution to notice the expected removal of H I prior to SF quenching.

- Higher redshift galaxies have higher H I-richness, which is independent of the radial distance to the main halo center of mass at higher redshift, but starts to be dependent on radius at lower redshift such that closer to the center the galaxies are less H I-rich. There is little to no radial dependence of the H I and H₂ contents of galaxies and their efficiency to convert into stars, and the gas consumption time remains unchanged with respect to the distance to the main halo at difference cosmic time explored here ($z \leq 2$).

- Galaxies can more efficiently convert H I-content into stars at lower redshift for more massive halo of infall. This scenario is not present for lower halo mass of infall. However, a general trend of higher efficiency of converting H I-content into stars in more massive halo of infall is apparent at all redshift except perhaps for the highest redshift ($z \sim 2$) that displays independent behaviour with respect to how big the virialised structure the galaxy falls in. H₂-richness as well as H₂-consumption time are not a function of the halo mass of infall. The higher H₂-richness and lower H₂-consumption time for higher redshift are barely visible at higher halo mass and even less at lower mass.

- Comparing to observations, qualitatively we agree with the trends in Wetzel et al. (2013) and Fossati et al. (2017) for a delayed-then-rapid quenching with $\tau_d \gg \tau_f$. However, the actual quenching

times (dominated by τ_d) are shorter by a factor of two in our simulations than inferred by Fossati et al. (2017). However, the work by Foltz et al. (2018) suggests a halo mass dependence of the quenching timescales with a range of < 1.5 Gyr which are more consistent with what our simulations predict, considering they only looked at cluster member galaxies.

Our results demonstrate that, within the group halo mass range simulated here, the delayed-then-rapid quenching of both star formation and neutral gas content within satellites is a natural outcome of the interplay between gas consumption and gas stripping within realistic haloes. The actual delay times at face value appear to be shorter than that inferred from observations, but in future work we will explore (via mocking up observational procedures) how the quenching timescales that are inferred from data compare to the timescales measured directly by tracking the simulated galaxies. Additionally, a proper statistical comparison would be greatly improved via a larger sample of zoom simulations, which are unfortunately quite computationally intensive. This preliminary work, nonetheless, demonstrates the power that cosmologically situated hydrodynamic models can yield valuable insights into the nature of satellite quenching.

ACKNOWLEDGEMENTS

MR and RD acknowledge support from the South African Research Chairs Initiative and the South African National Research Foundation. TN acknowledges support from the German Federal Ministry of Education and Research (BMBF) within the German-South-African collaboration project 01DG 15006. MR acknowledges financial support from Max-Planck-Institut für Astrophysik. Support for MR was also provided by the Square Kilometre Array post-graduate bursary program. The zoom simulations were run on DRACO which is part of the Max Planck Computing & Data Facility (<http://www.mpcdf.mpg.de>).

REFERENCES

- Agertz O., et al., 2007, *MNRAS*, **380**, 963
- Bower R. G., Benson A. J., Malbon R., Helly J. C., Frenk C. S., Baugh C. M., Cole S., Lacey C. G., 2006, *MNRAS*, **370**, 645
- Brammer G. B., et al., 2012, *ApJS*, **200**, 13
- Croton D. J., et al., 2006, *MNRAS*, **367**, 864
- Davé R., Thompson R., Hopkins P. F., 2016, *MNRAS*, **462**, 3265
- De Lucia G., Weinmann S., Poggianti B. M., Aragón-Salamanca A., Zaritsky D., 2012, *MNRAS*, **423**, 1277
- Faucher-Giguère C.-A., Kereš D., Dijkstra M., Hernquist L., Zaldarriaga M., 2010, *ApJ*, **725**, 633
- Foltz R., et al., 2018, preprint, ([arXiv:1803.03305](https://arxiv.org/abs/1803.03305))
- Fossati M., et al., 2017, *ApJ*, **835**, 153
- Gabor J. M., Davé R., 2015, *MNRAS*, **447**, 374
- Grogin N. A., et al., 2011, *ApJS*, **197**, 35
- Gunn J. E., Gott III J. R., 1972, *ApJ*, **176**, 1
- Hahn O., Abel T., 2011, *MNRAS*, **415**, 2101
- Hirschmann M., De Lucia G., Wilman D., Weinmann S., Iovino A., Cucciati O., Zibetti S., Villalobos Á., 2014, *MNRAS*, **444**, 2938
- Hopkins P. F., 2015, *MNRAS*, **450**, 53
- Hopkins P. F., Kereš D., Oñorbe J., Faucher-Giguère C.-A., Quataert E., Murray N., Bullock J. S., 2014, *MNRAS*, **445**, 581
- Hu C.-Y., Naab T., Walch S., Glover S. C. O., Clark P. C., 2016, *MNRAS*, **458**, 3528
- Kauffmann G., White S. D. M., Heckman T. M., Ménard B., Brinchmann J., Charlot S., Tremonti C., Brinkmann J., 2004, *MNRAS*, **353**, 713
- Kauffmann G., Li C., Zhang W., Weinmann S., 2013, *MNRAS*, **430**, 1447
- Kennicutt Jr. R. C., 1998, *ApJ*, **498**, 541
- Koekemoer A. M., et al., 2011, *ApJS*, **197**, 36
- Lacerna I., Contreras S., González R. E., Padilla N., Gonzalez-Perez V., 2018, *MNRAS*, **475**, 1177
- Larson R. B., Tinsley B. M., Caldwell C. N., 1980, *ApJ*, **237**, 692
- Lilly S. J., et al., 2007, *ApJS*, **172**, 70
- McGee S. L., Balogh M. L., Bower R. G., Font A. S., McCarthy I. G., 2009, *MNRAS*, **400**, 937
- Mitra S., Davé R., Finlator K., 2015, *MNRAS*, **452**, 1184
- Moster B. P., Naab T., White S. D. M., 2018, *MNRAS*, **477**, 1822
- Muratov A. L., Keres D., Faucher-Giguere C.-A., Hopkins P. F., Quataert E., Murray N., 2015, ArXiv e-prints:1501.03155,
- Naab T., Ostriker J. P., 2017, *ARA&A*, **55**, 59
- Oman K. A., Hudson M. J., 2016, *MNRAS*, **463**, 3083
- Oser L., Ostriker J. P., Naab T., Johansson P. H., Burkert A., 2010, *ApJ*, **725**, 2312
- Peng Y.-j., et al., 2010, *ApJ*, **721**, 193
- Planck et al., 2016, *A&A*, **594**, A13
- Rafieferantsoa M., Davé R., 2018, *MNRAS*, **475**, 955
- Rafieferantsoa M., Davé R., Anglés-Alcázar D., Katz N., Kollmeier J. A., Oppenheimer B. D., 2015, *MNRAS*, **453**, 3980
- Rahmati A., Pawlik A. H., Raičević M., Schaye J., 2013, *MNRAS*, **430**, 2427
- Schmidt M., 1959, *ApJ*, **129**, 243
- Simha V., Weinberg D. H., Davé R., Gnedin O. Y., Katz N., Kereš D., 2009, *MNRAS*, **399**, 650
- Somerville R. S., Davé R., 2015, *ARA&A*, **53**, 51
- Voit G. M., 2005, *Advances in Space Research*, **36**, 701
- Weinmann S. M., van den Bosch F. C., Yang X., Mo H. J., 2006, ArXiv Astrophysics e-prints,
- Wetzel A. R., Tinker J. L., Conroy C., van den Bosch F. C., 2013, *MNRAS*, **432**, 336
- Wetzel A. R., Tollerud E. J., Weisz D. R., 2015, *ApJ*, **808**, L27
- Wisnioski E., et al., 2015, *ApJ*, **799**, 209
- van Gorkom J. H., 2004, Clusters of Galaxies: Probes of Cosmological Structure and Galaxy Evolution, p. 305
- van Gorkom J. H., et al., 2003, *Ap&SS*, **285**, 219